Kalpa Publications in Computing

Volume 22, 2025, Pages 959–969

Proceedings of The Sixth International Conference on Civil and Building Engineering Informatics

Trans-Dimensional Statistical Inversion for Estimating Earth Pressures on Underground Structures

Zhiyao Tian[1] and Xianfei Yin[1]

[1] Department of Architecture and Civil Engineering, City University of Hong Kong, China.
zhiytian@cityu.edu.hk, xianfyin@cityu.edu.hk

Abstract

Identification of earth pressures acting on in-service underground structures is critical for their health monitoring and performance prediction. Given that the extensive deployment of sensors on poorly performing structures to measure pressure incurs high costs and presents technical challenges, the inversion of these pressures from easily observed deformation data has become increasingly desirable. However, traditional pressure inversion methods require subjective assumptions about the complexity of the pressure, necessitating extensive engineering judgment that may not be confidently applied in practice. To address this challenge, this paper proposes a trans-dimensional Bayesian method for pressure inversion. This method simultaneously incorporates pressure complexity and quantities into the inversion by parameterizing a set of previously unknown parameters, where the number of parameters itself is unknown. A recorded case study is presented for illustration and verification. It is found that the proposed method yields good inversion results on the pressures on a diaphragm wall, whereas traditional methods lead to poor inversion results due to inadequate assumptions. These outcomes highlight the advancements of the proposed method. Lastly, deficiencies and future extensions are discussed in the conclusion.

1 Introduction

With the rapid development of infrastructure construction, a wide range of underground structures have been put into service. However, the in-service environment of these structures is exceedingly complex (Yin et al., 2020; Tian et al., 2022). Factors such as extensive human engineering activities and unforeseen changes in geotechnical conditions can significantly disturb these structures, often resulting in performance deterioration that far exceeds initial design expectations (Zhou et al., 2020; Gong et al., 2023). This issue is well-documented by numerous practical cases (Van Empel et al. 2016; Bowers & Moss, 2018; Zhang et al., 2019); for instance, excessive deformations and serious

I. Hkust, J. Cheng and Y. Yantao (eds.), ICCBEI 2025 (Kalpa Publications in Computing, vol. 22), pp. 959–969

defects have been frequently observed in subway tunnel linings worldwide, particularly in cities characterized by soft soil conditions (Carpio et al., 2019; Tian et al., 2023a). Ensuring the operational safety of these infrastructures has emerged as a significant challenge for engineers.

Earth pressure acts as a mediator in the complex interactions between underground structures and the surrounding strata, playing a crucial role in influencing structural performance. Accurately identifying the current earth pressures is essential for the health monitoring and performance prediction of these in-service structures (Liu et al., 2016; Tian et al., 2023a). However, embedding sensors to monitor the pressures in structures that have already been cast and buried presents significant technical challenges (Zhou et al., 2024). Furthermore, the cost of equipping all newly built underground structures with sensors is prohibitively expensive (Zhou et al., 2021). Consequently, the inversion of earth pressures from easily observable structural responses, say deformations, has emerged as a more desirable approach.

Pressure inversion consists of two primary process, i) parametrization, i.e., use parameters to represent a priori unknown pressures; and ii) inference, i.e., deduce the values of these parameters from observed data to reconstruct the entire pressure distribution. A straightforward approach assumes earth pressures based on a predefined design mode, parameterizing the distributed pressures into specific parameters defined by the mode (e.g., $\mathbf{q}=(q_1, q_2, q_3)^T$ in Figure 1a), and then employing optimization methods to find solutions (values of $\mathbf{q}$) that yield structural responses closely aligned with the observed data (Yan et al., 2019).

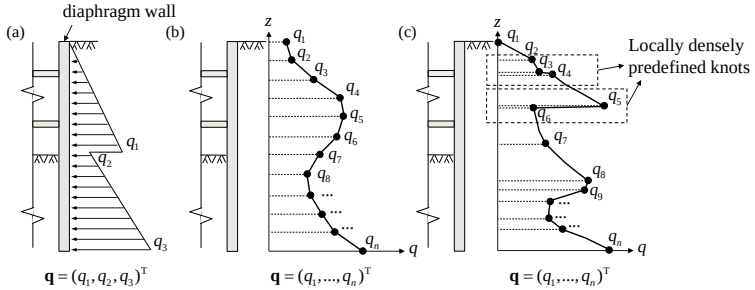

Figure 1: Schematic illustrating the parameterization of earth pressures on in-service underground structures: (a) parameterization based on a predefined design model; (b) parameterization utilizing an interpolation technique; (c) parameterization for complex pressure distributions exhibiting abrupt changes

However, due to the complex underground environment, earth pressures acting on in-service structures may distribute unevenly, often deviating significantly from the design mode. To address this, an interpolation technique has been proposed that parameterizes the unknown pressures using a set of unknown knots (e.g., $\mathbf{q}=(q_1, \ldots., q_n)^T$ in Figure 1b) (Gioda & Jurin, 1981). This interpolation approximates the unknown pressures, transforming the inversion of pressures into the inversion of the unknown knot parameters.

While this technique abandons strict design mode assumptions, it introduces two significant issues by expanding the parameter space: ill-conditioning and non-uniqueness (Sanchez & Benaroya, 2014). Specifically, minor errors in observed data can lead to substantial biases in inversion results (ill-conditioning), while vastly different pressures may yield similar structural responses (non-uniqueness). (Liu et al., 2019) and (Liu et al., 2021) observed these phenomena and employed regularization techniques to address ill-conditioning, achieving satisfactory inversion results. Additionally, (Tian et al. 2023b) and (Tian et al., 2024a) introduced a Bayesian approach capable of quantifying uncertainties associated with non-uniqueness, thereby informing the strategic addition of observations to mitigate non-uniqueness. Despite these advancements, a notable limitation persists: the complexity of pressure distributions must still be predefined. As indicated in Figure 1(b), the

number and locations of knots are assumed prior to inversion. For example, the unknown knots are typically assumed to be evenly distributed across the structural domain. However, for complex pressure distributions, as exemplified in Figure 1(c), abrupt changes in pressures necessitate densely predefined unknown knots locally for improved inversion outcomes. These assumptions require considerable engineering judgement, which may not always be confidently applied in practice.

To address this problem, this paper introduces a trans-dimensional Bayesian inversion approach that jointly incorporates the complexity and specific values of a priori unknown earth pressures into the inversion process, eliminating the need for preconceived assumptions and engineering judgment regarding pressure distribution. Section 2 details this method, while Sections 3–4 presents a numerical case to discuss the superiority of the proposed method. Deficiencies and future extensions are discussed in the conclusion.

2 THE TRANS-DIMENSIONAL BAYESIAN METHOD

2.1 Parameterization

Targeting the limitations of the methodologies previously discussed, an idea is proposed that why not integrates both pressure complexity and pressure values into the inversion process? To this end, a trans-dimensional parametrization method is introduced, as detailed below. As shown in Figure 2, z denotes a generalized coordinate on a structure, such as depth on a diaphragm wall or a polar angle on a shield tunnel ring. $q(z)$ represents the a priori unknown distributed earth pressures acting on the underground structure across the its domain. The parameterization of the earth pressure still employs an interpolation method using a set of knots. However, this method now incorporates the number of knots (n), the locations of the knots ($\mathbf{z}$, where $\mathbf{z}=(z_1,\ldots,z_n)^{\mathrm{T}}$), and the values at these knots ($\mathbf{q}$, where $\mathbf{q}=(q_1,\ldots,q_n)^{\mathrm{T}}$) jointly into the inversion process. The interpolation is performed using the interpolation function presented in Equation (1):

$$q(z)=\mathbf{I}(z)\mathbf{q} \tag{1}$$

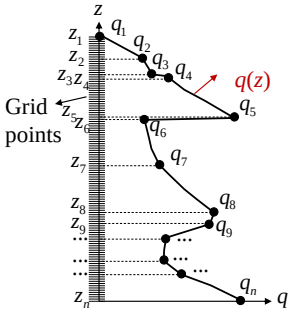

Figure 2: Schematic illustrating the trans-dimensional parameterization method

As a result, the inversion of the a priori unknown earth pressures $q(z)$ is transformed into the inversion of an unknown parameter set $\mathbf{m}$, where $\mathbf{m}=(n,\mathbf{z},\mathbf{q})$, and $\mathbf{I}(z)$ is the interpolation operator related to n and $\mathbf{z}$. A detailed derivation is presented in (Press, 2007). Regarding the unknown parameters, n is a discrete random variable taking values in $\mathbf{N}^{+}$; q_i (i=1,…,n) is a continuous random variable defined over $\mathbf{R}$; for mathematical convenience, z_i (i=1,…,n) is considered a discrete random variable taking values at grid points that are evenly distributed across the entire structural domain

(Figure 2). In practical applications, it is advisable to set the grid points as densely as possible, with subsequent case study potentially providing a reference for their specific configurations.

2.2 The Bayesian framework

The objective is the inference of the values of **m** given the observed structural deformations **d**. This inference is conducted within a Bayesian framework as represented by Equation (2):

$$p(\mathbf{m}|\mathbf{d}) \propto p(\mathbf{d}|\mathbf{m})\,p(\mathbf{m}), \tag{2}$$

where, $p(\mathbf{m}|\mathbf{d})$ is the posterior distribution, representing the statistical inference results of **m** given **d**; $p(\mathbf{d}|\mathbf{m})$ and $\mathbf{p}(\mathbf{m})$ represent the likelihood function and the prior distribution, respectively.

(1) Prior distribution

The prior distribution is further elaborated in Equation (3):

$$p(\mathbf{m}) = p(n)\,p(\mathbf{z}|n)\,p(\mathbf{q}|n,\mathbf{z}). \tag{3}$$

A Poisson distribution (with parameter λ) is employed to specify the prior for the number of parameters, i.e., $n \sim \text{Poisson}(\lambda)$. This prior effectively limits model complexity and aids in preventing overfitting (Denison et al., 1998). For clarity, let N_g denote the number of grid points across the structural domain. The prior for **z** given n is considered as placing n knots without replacement among the N_g points, with each point being selected with equal probability; The parameter **q** is assumed to follow a uniform distribution within the physically plausible range $[q_{\min}, q_{\max}]$, with mathematical details presented in Equation (4). This strategy allows the observed data to exert a more pronounced influence on the posterior distribution.

$$\begin{cases} p(n) = \dfrac{\lambda^n}{n!}e^{-\lambda} \\ p(\mathbf{z}|n) = \dfrac{1}{C_{N_g}^n} \\ p(\mathbf{q}|n,\mathbf{z}) = \displaystyle\prod_{i=1}^{n} p(q_i|n,z_i) = \prod_{i=1}^{n} \frac{1}{q_{\max}-q_{\min}} \end{cases}. \tag{4}$$

(2) Likelihood function

The likelihood function quantifies the fit between observed structural responses and those predicted by $g(q(z))$. In line with the Central Limit Theorem, the likelihood function is generally assumed to follow a zero-mean Gaussian distribution, as shown in Equation (5):

$$p(\mathbf{d}|\mathbf{m}) = \frac{1}{(2\pi\sigma_{\mathrm{d}}^2)^{l/2}} \exp\{-\frac{[\mathbf{d}-g(q(z))]^{\mathrm{T}}[\mathbf{d}-g(q(z))]}{2\sigma_{\mathrm{d}}^2}\}, \tag{5}$$

where, σ_{d} is the expected standard deviation, measuring the dispersion between observed and predicted structural responses; $g(q(z))$, also referred to as the load-structure model, computes the structural responses under earth pressure q(z), determined by the parameter set m. Given the potential complexity of the distribution, the Finite Element Method (FEM) can be utilized to construct the forward model, detailed in Equation (6):

$$g(q(z)) = g(\mathbf{I}(z)\mathbf{q}) = \mathbf{K}^{-1}\mathbf{f}(\mathbf{I}(z)\mathbf{q}), \tag{6}$$

where, the structure is discretized into a series of elements, with **K** representing the global stiffness matrix; **f** being a vector-valued function where $\mathbf{f}(\mathbf{I}(z)\mathbf{q})$ denotes the equivalent global forces equivalent

to the distributed pressure $\mathbf{I}(z)\mathbf{q}$, adhering to the transformation rules of virtual work. For a detailed derivation of $\mathbf{K}$ and $\mathbf{f}$ regarding typical underground structures such as piles and tunnels, the reader is referred to (Tian et al., 2023b) and (Tian et al., 2024a).

2.3 The Markov chain

Directly substituting Equations (3)–(6) into Equation (2) to derive an analytical solution is impractical. Instead, the Markov Chain Monte Carlo (MCMC) method provides a numerical approach for sampling the posterior distribution. A trans-dimensional MCMC method is proposed by presented. Green (1995), which tackles the above-mentioned trans-dimensional problems by establishing the detailed balance condition for trans-dimensional parameters, as shown in Equation (7):

$$p(\mathbf{m}^*|\mathbf{d})Q(\mathbf{m}^*|\mathbf{m}_c)\alpha(\mathbf{m}^*|\mathbf{m}_c) = p(\mathbf{m}_c|\mathbf{d})Q(\mathbf{m}_c|\mathbf{m}^*)\alpha(\mathbf{m}_c|\mathbf{m}^*)|\mathbf{J}|, \tag{7}$$

where, $Q(.)$ is the proposal function, e.g., generating candidate parameters $\mathbf{m}^*$ from the current state $\mathbf{m}_c$; $\alpha(.)$ represents the acceptance ratio; $\mathbf{J}$ is the Jacobian matrix for the diffeomorphism from $\mathbf{m}_c$ to $\mathbf{m}^*$. This setup enables the design of a proposal function that facilitates transitions between different dimensions, leading to the derivation of the necessary acceptance ratio (Equation (8)) for constructing a trans-dimensional Markov chain:

$$\alpha(\mathbf{m}^*|\mathbf{m}_c) = \min\{1, \frac{p(\mathbf{m}_c|\mathbf{d})Q(\mathbf{m}_c|\mathbf{m}^*)}{p(\mathbf{m}^*|\mathbf{d})Q(\mathbf{m}^*|\mathbf{m}_c)}|\mathbf{J}|\}. \tag{8}$$

Equation (9) shows the expansion of the proposal function. Following the principles outlined by (Green, 1995), we have developed subsequent proposal functions for addressing the earth pressure inversion problem, based on the three components of Equation (9). Specifically, each iteration of the chain involves proposing three types of proposals—birth, death, and move—with equal probability. These steps enable transitions between different parameter dimensions, as indicated in Equation (10):

$$Q(\mathbf{m}^*|\mathbf{m}_c)=Q(n^*,\mathbf{z}^*,\mathbf{q}^*|n_c,\mathbf{z}_c,\mathbf{q}_c)= Q(n^*|n_c,\mathbf{z}_c,\mathbf{q}_c)Q(\mathbf{z}^*|n_c,\mathbf{z}_c,\mathbf{q}_c,n^*)Q(\mathbf{q}^*|n_c,\mathbf{z}_c,\mathbf{q}_c,n^*,\mathbf{z}^*) \tag{9}$$

$$Q(n^*|n_c,\mathbf{z}_c,\mathbf{q}_c) = Q(n^*|n_c) = \begin{cases} 1/3 & n^* = n_c+1, \text{ birth} \\ 1/3 & n^* = n_c-1, \text{ death} \\ 1/3 & n^* = n_c, \quad \text{move} \end{cases}. \tag{10}$$

i) Birth step: randomly add a new knot z_b randomly at a candidate point previously unoccupied; and assign a value q_b to this new knot according to Equation (11); ii) Death step: the reverse step of Birth, namely randomly choose one existing knot randomly to delete (Equation 12); and iii) Move step: propose a Gaussian perturbation for the current values $\mathbf{q}_c$, following $N(\mathbf{q}_c, \mathbf{C}_m)$, where $\mathbf{C}_m$ is the covariance matrix for the proposal (Equation 13):

$$\begin{cases} Q_{Birth}(\mathbf{z}^*|n_c,\mathbf{z}_c,\mathbf{q}_c,n^*) = Q(z_b|n,\mathbf{z}) = \dfrac{1}{C_{N_g-n}^1} = \dfrac{1}{N_g-n} \\ Q_{Birth}(\mathbf{q}^*|n_c,\mathbf{z}_c,\mathbf{q}_c,n^*,\mathbf{z}^*) = Q(q_b|q_p) = \dfrac{1}{(2\pi\sigma_b^2)^{1/2}}\exp[-\dfrac{(q_b-q_p)^2}{2\sigma_b^2}] \end{cases}. \tag{11}$$

$$\begin{cases} Q_{Death}(\mathbf{z}^*|n_c,\mathbf{z}_c,\mathbf{q}_c,n^*) = Q(z_d|\mathbf{z}) = \dfrac{1}{C_n^1} = \dfrac{1}{n} \\ Q_{Death}(\mathbf{q}^*|n_c,\mathbf{z}_c,\mathbf{q}_c,n^*,\mathbf{z}^*) = Q(q_b|z_d) = 1 \end{cases}. \tag{12}$$

$$\begin{cases} Q_{Move}(\mathbf{z}^* \,|\, n_c, \mathbf{z}_c, \mathbf{q}_c, n^*) = 1 \\ Q_{Move}(\mathbf{q}^* \,|\, n_c, \mathbf{z}_c, \mathbf{q}_c, n^*, \mathbf{z}^*) = Q(\mathbf{q}^* \,|\, \mathbf{q}_c) = \dfrac{1}{(2\pi)^{\frac{n}{2}} |\mathbf{C}_m|^{1/2}} \exp[-\dfrac{1}{2}(\mathbf{q}^* - \mathbf{q})^T \mathbf{C}_m^{-1}(\mathbf{q}^* - \mathbf{q})] \end{cases} \quad (13)$$

It is important to note that the birth step is the inverse of the death step. By incorporating Equations (9) –(13) into Equation (8), the acceptance ratios for birth, move, and death steps are derived as Equations (14)–(16):

$$\alpha_{Birth}(\mathbf{m}^* \,|\, \mathbf{m}_c) = \min\{1, \frac{p(\mathbf{d}|\mathbf{m}^*)}{p(\mathbf{d}|\mathbf{m}_c)} \frac{1}{Q(q_b \,|\, q_p)} \frac{\lambda/(n+1)}{q_{\max} - q_{\min}}\} \quad (14)$$

$$\alpha_{Death}(\mathbf{m}^* \,|\, \mathbf{m}_c) = \min\{1, \frac{p(\mathbf{d}|\mathbf{m}^*)}{p(\mathbf{d}|\mathbf{m}_c)} Q(q_b \,|\, q_p) \frac{(q_{\max} - q_{\min})}{\lambda/n}\} \quad (15)$$

$$\alpha_{Move}(\mathbf{m}^* \,|\, \mathbf{m}_c) = \min\{1, \frac{p(\mathbf{d}|\mathbf{m}^*)}{p(\mathbf{d}|\mathbf{m}_c)}\}. \quad (16)$$

The Markov chain operates by selecting, with equal probability, to proceed with birth, death, or move processes at each step. For enhanced optimization of convergence speed, readers are directed to the adaptive reversible jump MCMC algorithm proposed by the authors (Tian et al., 2024b) which includes ready-to-use attached codes.

3 CASE STUDY

3.1 Background

A case study introduced by (Tian et al., 2023b) is utilized to apply and verify the proposed method. Notably, in this case, the authors manually adding densely interpolated knots at locations prone to abrupt pressure changes. In this paper, we will demonstrate that our method is able to incorporate pressure complexity into the inversion process, eliminating the need for potentially subjective pre-assumptions. As shown in Figure 3(a), A diaphragm wall bent towards a pit due to the active earth pressures behind it. Engineers recorded the deformations of the wall, inclusive of potential measurement errors, as shown in Figure 3(b). Consequently, the objective herein is the inversion of earth pressures using the deformation data.

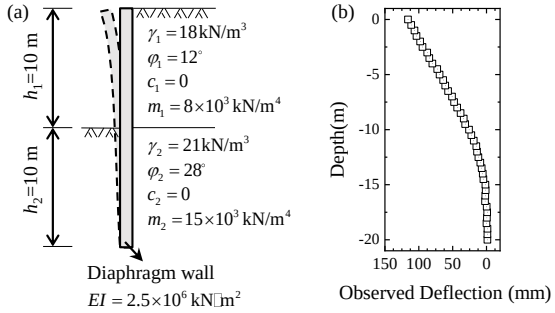

Figure 3: The case study: (a) a diaphragm wall bent towards a pit; (b) deformation data. (Note: γ, φ, c, and m represent the unit weight, friction angle, cohesion, and foundation stiffness scaling factor of the soil, respectively; EI is the bending rigidity of the wall)

The structural domain extends from 0 to 20 m. A dense grid of points is established across this domain, with a spacing of 10 points per meter, resulting in N_g = 201. The interpolation method with parameter set **m**, **m**=(n, **z**, **q**) is employed for parameterization. The prior for n is defined as n ~ Poisson (31), where λ=31 is chosen somewhat arbitrarily, awaiting updates from observed data; The prior for **z** is specified as p(**z**|n)=1/C(N_g,n); The prior for **q** is set as **q**|n,**z** ~ Uniform(0, 400). This decision is based on the assumption that the soil cannot exert any traction, and that 400 kPa is a substantially large value for the active pressures in this case. The "beam on elastic foundation" model is utilized to construct the forward model g(.), with parameters shown in Figure 3. The standard error in deformation measurement, σ_d is set as 1 mm for the likelihood function. Consequently, the prior (Equation 4) and likelihood function (Equation 5) have been established. The adaptive reversible jump MCMC algorithm (Tian et al., 2024b) is then employed to estimate the posterior distribution.

3.2 Results

The established Markov chain progressed through 10^6 steps. The log likelihood (LL) of the chain, together with the parameter n, is presented in Figure 4. As shown in Figure 4 (a), LL rapidly converges from a very low initial value and stabilizes around –20. n jumps between 4 and 45 throughout the chain, indicating the chain's ability to sample parameters across various dimensions. Particularly in the second half of the chain, the behaviors of LL and n resemble white noise, suggesting convergence of the Markov chain. Consequently, samples from this second half were then used to estimate the posterior distribution of earth pressures.

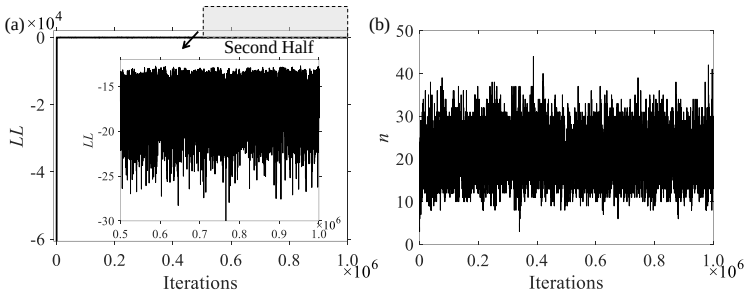

Figure 4: The established Markov chain: (a) the log likelihood (LL) along the chain; (b) n along the chain

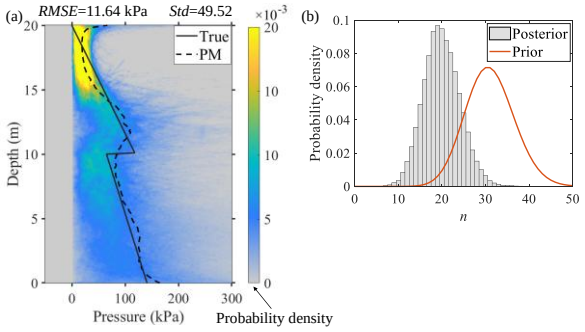

Figure 5: Inversion results: (a) the posterior distribution of earth pressures; (b) the posterior distribution of n

The inversion results are presented in Figure 5. Figure 5(a) illustrates the posterior distribution of earth pressures, where lighter colors signify higher probabilities, and darker colors indicate lower probabilities. The true pressures, also displayed in this figure, are predominantly confined within zones of high probability, which underscores the effectiveness of the proposed method. In addition, the posterior mean (PM) is a representative solution of the posterior distribution. It is evident that the PM aligns closely with the actual pressures, achieving an RMSE of 11.64 kPa, thus reaffirming the method's efficacy. Additionally, the standard deviation (Std) serves as an index to quantify the uncertainty of these results, with further details to be explored in subsequent discussions. As demonstrated in Figure 5(b), the initial prior distribution for *n* centered at 31, subsequently updated to center around 19, suggests that the method can automatically infer the complexity of pressures based on observed deformation data. This advancement will be discussed in detail in the next section.

4 Discussion

4.1 Advancement of the proposed method

This section will illustrate the essentiality of incorporating pressure complexity into inversion processes. It is important to reemphasize that in the discussed case study, (Tian et al. 2023b) pre-assumed pressure complexity by manually adding densely interpolated knots at locations prone to abrupt pressure changes. However, in engineering practice, pressure is unknown *a priori*, and engineers have limited information about where to insert such knots. Alternatively, one might consider a method of distributing knots evenly, and progressively densifying them as demonstrated in Figures. 6(a)–(c). With a sufficient density of knots, there may no longer be a need to presuppose pressure complexity. This strategy could potentially serve as an alternative to the method proposed herein. To validate its efficacy, comparative tests with the proposed method are conducted as follows.

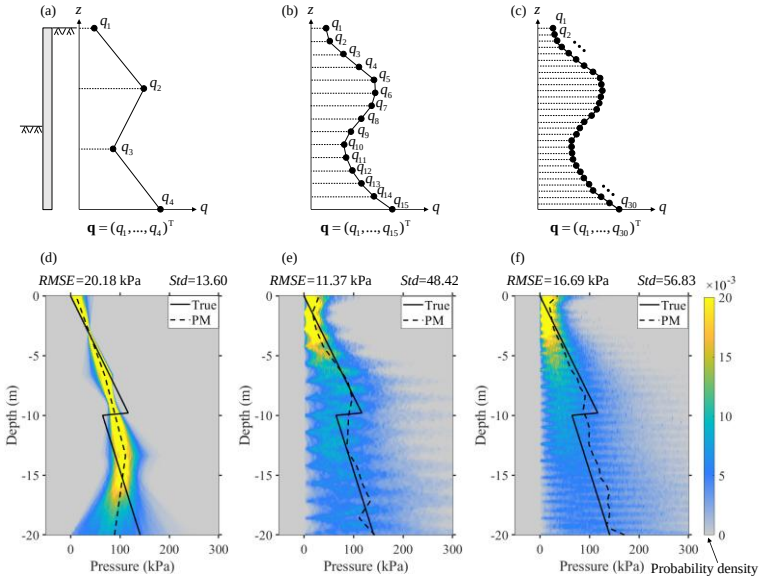

Figure 6: Parameters settings and results for the fixed-dimensional Bayesian method: (a) 4 parameters; (b) 15 parameters (c) 30 parameters; (d-f) corresponding results for 4, 15, and 30 parameters, respectively.

Additional experiments were carried out. As illustrated in Figures. 6(a)–(c), earth pressures were parameterized into a set of evenly distributed interpolated knots. The objective was the inversion of fixed parameters **q**, where $\mathbf{q}=(q_1,\ldots,q_n)^T$ with n=4, 15, and 30, for the three additional cases, respectively. These experiments utilized the fixed Bayesian method as introduced by (Tian et al., 2023b). The results are presented in Figures. 7(d)–(e), and are compared with the outcomes obtained using the proposed method (Figure. 5).

As indicated in Figure. 6(d), when the number of parameters is fixed at 4, the inversion results are poor, with RMSE being 20.18 kPa; When n increases to 15, the inversion results improve with RMSE being 11.37 kPa; However, increasing n to 30 results in poorer outcomes, with RMSE increasing to 16.69 kPa. The underlying mechanism can be explained by the fact that with a small number of parameters, the pre-assumed pressure complexity is insufficient to capture the real distributed pressures. As the number of parameters increases, the method's ability to approximate actual pressure distributions improves. However, when there are too many parameters, the available deformation data may not be informative enough to infer such a large number of unknowns, leading to increased uncertainty and deteriorated results. This is also evident in the index, *Std*, which grows from 13.60 to 48.42, to 56.83, illustrating an increase in the uncertainties associated with the inversion results across the three experiments. Although an RMSE suggests that the fixed-dimensional method with 15 parameters marginally outperforms the proposed method (Figure 5), in engineering practice, there are no "true" pressures available to fine-tune these parameters. Unlike the fixed-dimensional approach, the proposed method does not require an assumption of the pressure complexity, underscoring its advancement and applicability.

4.2 Limitations and future extensions

It is worth noting that this paper primarily illustrates the application of the proposed method to diaphragm walls. As highlighted in the Introduction, the potential extension of this method to tunnels or pipelines is of particular interest due to the pronounced structural deterioration. However, such an extension may encounter substantial technical challenges. Specifically, the inversion process necessitates numerous iterations of the trans-dimensional chain on the mechanical model, $g(.)$. In this illustrative example, $g(.)$ is simplified as a linear-elastic model for the diaphragm wall. However, when attempting to extend this method to tunnels or pipelines, the structural behavior may exhibit highly nonlinear characteristics, especially in the large deformation stage. Accordingly, the total number of iterations required to solve the nonlinear mechanical model via multiple Markov chain iterations may introduce an extensive computational burden. As expected, when extending to nonlinear cases, the time required will multiply with the increase in iterations needed to solve the nonlinear mechanical model.

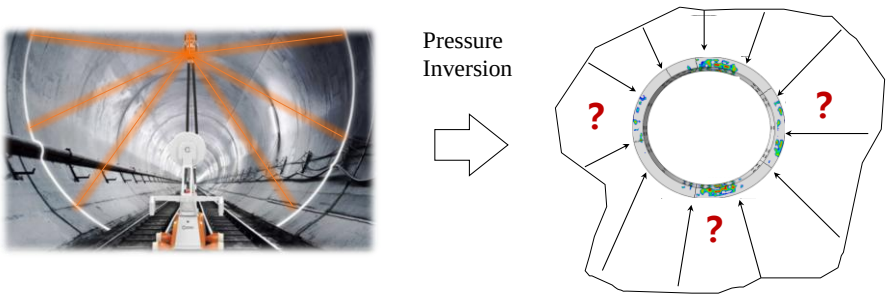

Figure 7: Expected extensions to tunnels and pipelines to assist in structural health monitoring.

Despite these challenges, such an extension remains highly attractive. As illustrated in Figure 7, utilizing a laser scanner to acquire deformation data (**d**) on these structures facilitates the inversion of earth pressures ($q(z)$) with the proposed method. Upon identifying the critical factors—specifically, earth pressure—influencing structural performance, $g(.)$ can be "driven" once again. This enables the execution of a real-time simulation, $\mathbf{D}=g(q(z))$, to develop a mechanical digital twin model for these in-service and poorly performing structures. Such a model aids in structural health monitoring by providing comprehensive simulation outputs, including stress and damage profiles, which warrants further research in the future.

5 Conclusions

A trans-dimensional Bayesian load inversion method is proposed to infer earth pressures on in-service underground structures using easily observable deformation data. The distinctive feature of this method, compared to state-of-the-art approaches, is its trans-dimensional framework, which facilitates the incorporation of load complexity into the inversion process.

A case study is presented to illustrate its advancements and potential: traditional methods require a pre-assumption of pressure complexity, and inadequate assumptions can lead to poor inversion results that fail to identify true pressures. In contrast, the proposed method adaptively infers both the complexity and quantity of pressures, achieving satisfactory inversion outcomes without reliance on subjective assumptions.

This paper demonstrates the proposed method on a diaphragm wall as an example. Expanding this approach to tunnels and pipelines is of great interest and could lead to mechanical digital twins for these structures. Due to length constraints, a more detailed exploration, rigorous validation, and discussion of uncertainty will be presented in future publications.

Acknowledgement

The authors acknowledge the supports from Natural Science Foundation of China (Grant No. 72404233) and Guangdong Basic and Applied Basic Research Foundation (2025A1515010190).

References

Bowers, K., & Moss, N. (2018). Investigation and reconstruction of a London Underground tunnel, UK. Proceedings of The Institution of Civil Engineers-Civil Engineering, 171(1): 43-48.

Carpio, F., Peña, F., & Galván, A. (2019). Recommended deformation limits for the structural design of segmental tunnels built in soft soil. Tunnelling and Underground Space Technology, 90, 264-276.

Denison, D. G. T., Mallick, B. K., & Smith, A. F. M. (1998). Automatic Bayesian curve fitting. Journal of the Royal Statistical Society, 60(2), 333-350.

Gioda, G., & Jurina, L. (1981). Numerical identification of soil‐structure interaction pressures. International Journal for Numerical and Analytical Methods in Geomechanics, 5(1), 33-56.

Gong, Q., Hui, X., & Tian, Z. (2023). Risk section classification of tunnel settlement based on land-use development simulation and uncertainty analysis. International journal of transportation science and technology, 12(3), 716-728.

Green, P. J. (1995). Reversible jump Markov chain Monte Carlo computation and Bayesian model determination. Biometrika, 82(4), 711-732.

Liu, Q., Liu, H., Huang, X., Pan, Y., Luo, C., & Sang, H. (2019). Inverse analysis approach to identify the loads on the external TBM shield surface and its application. Rock Mechanics and Rock Engineering, 52, 3241-3260.

Liu, H., Liu, Q., Liu, B., Tang, X., Ma, H., Pan, Y., & Fish, J. (2021). An efficient and robust method for structural distributed load identification based on mesh superposition approach. Mechanical Systems and Signal Processing, 151, 107383.

Liu, X., Bai, Y., Yuan, Y., & Mang, H. A. (2016). Experimental investigation of the ultimate bearing capacity of continuously jointed segmental tunnel linings. Structure and Infrastructure Engineering, 12(10), 1364-1379.

Press, W. H. (2007). Numerical Recipes: The Art of Scientific Computing (3rd ed.). Cambridge University Press.

Sanchez, J., & Benaroya, H. (2014). Review of force reconstruction techniques. Journal of Sound and Vibration, 333(14), 2999-3018.

Tian, Z., Gong, Q., Di, H., Zhao, Y., & Zhou, S. (2022). What causes the excessive metro tunnel settlement in soft deposits: learned from a detailed case with factor decomposition. Bulletin of Engineering Geology and the Environment, 81(5), 212.

Tian, Z., Xu, P., Gong, Q., Zhao, Y., & Zhou, S. (2023a). Health-degree model for stagger-joint-assembled shield tunnel linings based on diametral deformation in soft-soil areas. Journal of Performance of Constructed Facilities, 37(3), 04023019.

Tian, Z., Zhou, S., Lee, A., Zhao, Y., & Gong, Q. (2023b). A Bayesian-based approach for inversion of earth pressures on in-service underground structures. Acta Geotechnica, 19(4), 1911-1928.

Tian, Z., Zhou, S., Lee, A., Shan, Y., & Detmann, B. (2024a). How to identify earth pressures on in-service tunnel linings: Insights from Bayesian inversion to address non-uniqueness. Transportation Geotechnics, 48, 101344.

Tian, Z., Lee, A., & Zhou, S. (2024b). Adaptive tempered reversible jump algorithm for Bayesian curve fitting. Inverse Problems, 40(4), 045024.

Van Empel, W. H. N. C., Sip, J. W., & Haring, F. P. (2006). Design of repair measures of a damaged shield driven tunnel. Tunnelling and Underground Space Technology, 21(3), 338-339.

Yan, Q., Zhang, W., Zhang, C., Chen, H., Dai, Y., & Zhou, H. (2019). Back analysis of water and earth loads on shield tunnel and structure ultimate limit state assessment: a case study. Arabian Journal for Science and Engineering, 44, 4839-4853.

Yin, X., Liu, H., Chen, Y., Wang, Y., & Al-Hussein, M. (2020). A BIM-based framework for operation and maintenance of utility tunnels. Tunnelling and Underground Space Technology, 97, 103252.

Zhang, D. M., Liu, Z. S., Wang, R. L., & Zhang, D. M. (2019). Influence of grouting on rehabilitation of an over-deformed operating shield tunnel lining in soft clay. Acta Geotechnica, 14(4), 1227-1247.

Zhou, S., Jin, Y., Tian, Z., Zou, C., Zhao, H., & Miao, Z. (2024). Exploring the feasibility of prestressed anchor cables as an alternative to temporary support in the excavation of super-large-span tunnel. Railway Engineering Science, 32, 344-360.

Zhou, S., Tian, Z., Di, H., Guo, P., & Fu, L. (2020). Investigation of a loess-mudstone landslide and the induced structural damage in a high-speed railway tunnel. Bulletin of Engineering Geology and the Environment, 79, 2201-2212.

Zhou, Z., Chen, Z., He, C., & Kou, H. (2021). Investigation on the evolution characteristics and transfer mechanism of surrounding rock pressure for a hard-rock tunnel under high geo-stress: case study on the Erlang Mountain Tunnel, China. Bulletin of Engineering Geology and the Environment, 80(11), 8339-8361.